Investigating small RPAS ground impact injury severity criteria: phase 2

Sagar, MD Farhan Hoque; Gunasekaran, Kalish; Bian, Kewei; Potts, Emilie; Islam, Sakib Ul; Gholipour, Javad; Vidal, Charles; Mao, Haojie

For the publisher's version, please access the DOI link below./ Pour consulter la version de l'éditeur, utilisez le lien DOI ci-dessous.

https://doi.org/10.4224/40003280

Investigating small RPAS Ground Impact Injury Severity Criteria
Phase 2

MD Farhan Hoque Sagar[1], Kalish Gunasekaran[1], Kewei Bian[1], Emilie Potts[1], Sakib Ul Islam[1], Javad Gholipour[2], Charles Vidal[2] and Haojie Mao[1,3]

1 Mechanical and Materials Engineering, Faculty of Engineering, Western University, London, Ontario, Canada

2 National Research Council Canada – Aerospace Research Center, 2107 Chemin de la Polytechnique, Montréal Québec, Canada H3T 1J4

3 School of Biomedical Engineering, Western University, London, Ontario, Canada

Table of contents

LIST OF FIGURES

List of tables

ABSTRACT

The overarching goal of Phase 2 of this project was focused on investigating small remotely piloted aircraft (sRPA) to human head impact safety. Previously, a finite element (FE) model of a representative quadcopter sRPA was developed and was used to study sRPA impacts to the human head. In this phase of the project, we intended to further validate the small female human head-neck model, investigate head responses of children, and develop a new sRPA model to study head responses during the impacts with this sRPA model.

This Phase 2 report is focused on 1) describing the development and validation of a new sRPA model, 2) understanding the effect of impact velocity and kinetic energy using a wood block model, and especially 3) providing comprehensive data comparing head responses for various populations under impacts with two different types of sRPA. In brief, it was found that population variances and sRPA types greatly affected head responses, and the detailed responses were investigated and documented in this report.

Keywords: sRPAS, UAS, UAV, Drone, Head impact, Safety, Finite Element, Small female, Children

1 INTRODUCTION

With the detailed human head skull stress and brain strain during sRPA-to-head impacts being studied in Phase 1 of this study (1, 2), we now address the following question: how do sRPA of various structures and masses affect head responses? Such knowledge is needed to understand sRPA ground impact injury severity, and then better guide safety regulations which are applied to various sRPA types, masses, and structures. Meanwhile, cadaveric studies of sRPA to human impacts were reported (3). Especially, DJI Mavic Pro to cadaveric head impacts were conducted and head linear and rotational kinematics were reported (3), providing a unique opportunity to develop and validate a new finite element sRPA model. Hence, in this brief report, we describe our efforts in developing a new DJI Mavic Pro finite element (FE) model and validation of the model against cadaveric data.

2 METHODS

2.1 DJI Mavic Pro Model Development

2.1.1 DJI Mavic Pro Model Development

Mesh development
The DJI Mavic Pro FE model was meshed using HyperMesh (Altair, Troy, MI, USA), with the frame and battery components being separate. Spotwelds were used to connect the different parts. The arm joint with the main frame was one complicated part of this model. The arm of the actual DJI Mavic Pro is hinged and can rotate to a certain extent. Hence, a numerical revolute joint was defined to reinforce the connection between the frame and the arms. This numerical joint is a function defined in Ls-Dyna and specifies the revolution axis and the stiffness. The revolute joint was modelled for four sRPA arms to better represent these features in the FE model, allowing the arms of the sRPA to be flexible and rotate about the z axis (**Figure 1**).

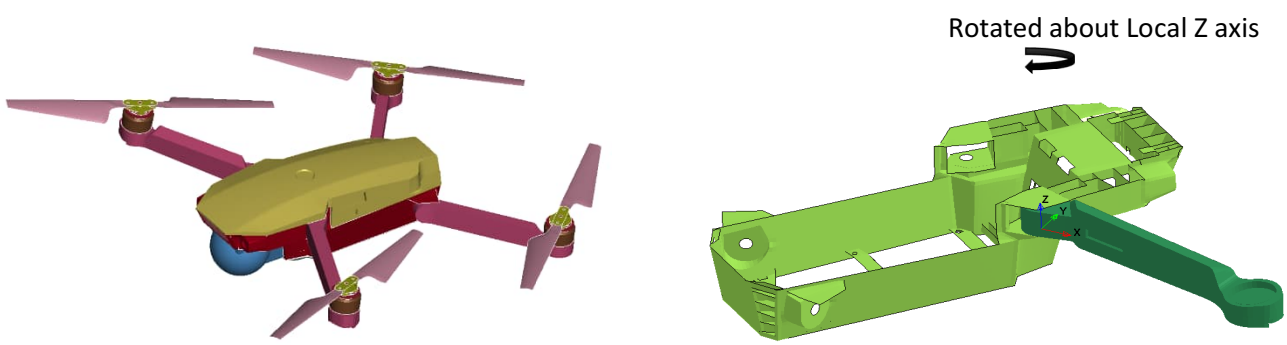

Figure 1: DJI Mavic Pro FE model and Frame & Arm connection

Material properties and element thickness

Based on the material information from the ASSURE report (3), which is presented in **Table 1**, the material properties of various components of the DJI Mavic Pro FE model were determined. Polycarbonate material was assigned to the body frame, upper & lower chassis, arm and propeller blades. The gimbal cover was first modeled using G10 fiberglass. However, this cover model was removed when simulating sRPA-to-head impacts, to mimic the real flight condition. The motor casing, clamp & blade hub were modeled using Case Aluminum 520F. Motor internal components were modeled using Steel 4030 for simplicity to represent a combination of magnet and copper wires.

The sRPA frame shell was deemed as the most important part because it makes direct contact with the human head during an impact. The energy of the moving sRPA would be transferred from the body shell to the head. As a result, the material properties of the shell were believed to play a significant role in the impact simulations. In general, the shell was made of polycarbonate plastic, a strong and durable material commonly used in engineering structures. According to the ASSURE report, the Johnson-Cook model was found to be suitable for simulating shells. **Table 3** summarizes the material properties of polycarbonate based on the ASSURE report.

Table 1: Material Properties

sRPA Parts	Material
Frame	Polycarbonate
Upper & Lower Chassis	Polycarbonate
Arm	Polycarbonate
Propeller Blades	Polycarbonate
Battery Pack	Battery (see Table 2)
Motor Casing	Case Aluminum 520F
Clamp	Case Aluminum 520F
Motor Internal Component	Steel 4030

Table 2: General Material Properties

Material	Young's modulus (MPa)	Poisson's ratio	Density (kg/m^3)
Cast Aluminum 520F	66,600	0.33	2,870
Steel 4030	200,500	0.29	8,650
G10 Fiber glass	13,790	0.12	1,980
Battery	500	0.33	5,477

Table 3: Polycarbonate material referred from the ASSURE

Density (kg/m^3)	Young's Modulus (GPa)	Shear Modulus (GPa)	A (MPa)	B (MPa)	C	M	N	C_v (KJ/kgK)	T_{melt} (K)
1197.8	2.59	0.93	80	75	0.0052	0.548	2	1.3	562

Note: A, B, C, M and N are input constants for Johnson and Cook flow stress equation.

2.1.2 Experimental Data Available for Validation

For the DJI Mavic Pro, there were a total of four (male) cadaveric experiments that were reported in the ASSURE Report. These cadaveric tests were focused on frontal and 58-degree impacts (**Table *4***). The 58 degree is the angle between the impact direction and the horizontal plane.

Table 4: Cadaveric experiment

Test #	sRPA	Impact Angle (deg)	Impact Direction	Speed (ft/s)
OSU #29	DJI Mavic Pro	58	Front	71
OSU #21	DJI Mavic Pro	58	Front	71
OSU #20	DJI Mavic Pro	58	Front	61
OSU #28	DJI Mavic Pro	58	Front	61

Note: The test # is referring directly to the ASSURE report naming convention.

The linear accelerations of cadaver heads demonstrated a relatively consistent pattern with distributed peak linear acceleration values and some impacts showing a lower-magnitude second peak (**Figure 2**). Head rotational velocities demonstrated two very distinctive patterns as one shows a double-peak pattern while the other shows shown a single peak pattern with peak values being about two times of the other two (**Figure 3**). These curves were extracted from the ASSURE report and then digitized to be compared to simulation data.

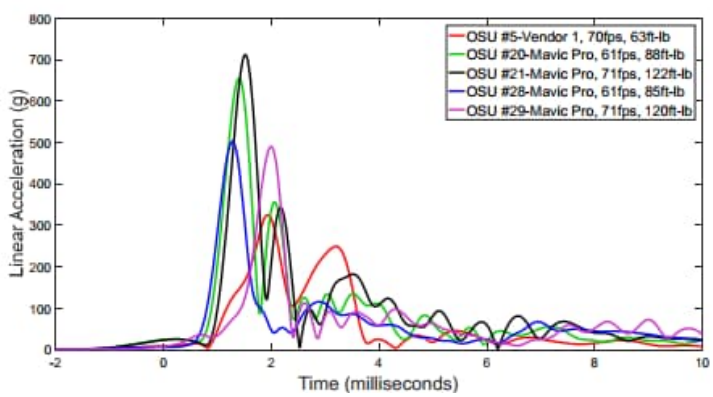

Figure 2: Head linear acceleration time histories in 58-degree, DJI Mavic Pro frontal impact scenarios (Experimental data from ASSURE)

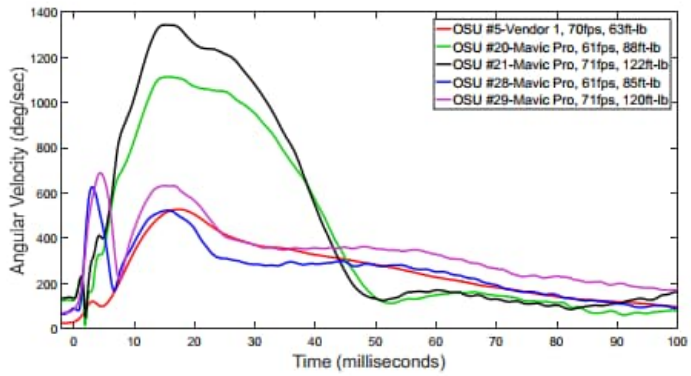

Figure 3: Head resultant angular velocity time histories in 58-degree, DJI Mavic Pro frontal impact scenarios (Experimental data from ASSURE)

2.1.3 DJI Mavic Pro FE Model Validation

Both HyperMesh and LS-PrePost (LSTC/ANSYS, Livermore, CA, USA) were used for the DJI Mavic Pro model and THUMS model integration during the preprocessing stage. Initial boundary and loading conditions included positioning the DJI Mavic Pro FE model relative to the human head according to the experimental setting (**Table *5***). The DJI Mavic Pro approach speeds (used in the FE model) were based on the experimental data. The contact condition between the sRPA and the human head was defined. For the DJI Mavic Pro model, the Frontal 58-degree scenario was employed. A numerical initial velocity in LS-DYNA was assigned to the sRPA. A numerical contact was then defined between the sRPA and human head model. The numerical accelerometers were defined on the human head model to collect linear acceleration and rotational velocity at head center of gravity following local coordinates. It was found that the Ls-PrePost would generate resultant linear accelerations with artificially high values for a later time stage. In order to accurately calculate the linear acceleration time histories, the x, y, and z axes linear acceleration data were first individually filtered with a low-pass CFC (channel frequency class) 1000 Hz filter and then resultant acceleration was calculated from the filtered x, y, and z data. Rotational velocities were filtered using the 180 Hz filter.

Table 5: Experimental Setting for Validation

Case #	Impact Direction	Impact Angle (deg)	Sex	Impact Velocity (m/s (ft/s))	Cadaver subject (see Table 6)
1	Frontal	58	Male	18.6 (61)	4
2	Frontal	58	Male	21.6 (71)	3
3	Frontal	58	Male	18.6 (61)	4
4	Frontal	58	Male	21.6 (71)	3

Toyota's Total Human Model for Safety (THUMS) average male model was used to investigate head responses (**Figure 4**).

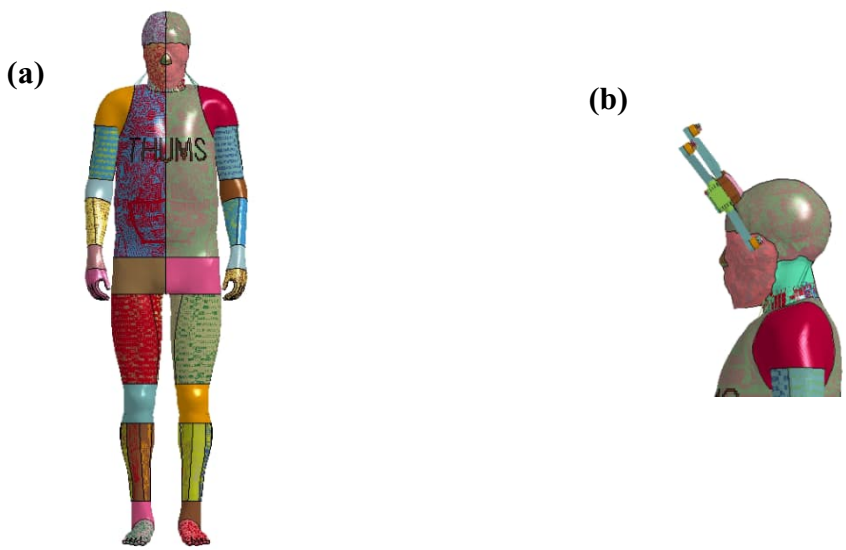

Figure 4: THUMS version 4.02 50 Percentile model. (a) Full model (b) Frontal 58-degree impact

2.1.4 Description of scaling for simulation validation

In the postmortem human subjects (PMHS) examinations, only the masses of complete subjects were reported. Two separate subjects, each with a different mass, were used in the experimental study. The whole-body masses were applied to calculate the scaling factors. **Table 6** summarizes the detailed information of subjects used in the Ohio State University (OSU) PMHS experiments, including subject's age, body mass and standing height.

Table 6: PMHS subjects

Subject	Age	Standing Height (inch)	Body Mass (lb)
3	67	71	143
4	67	72	193
5	74	74	195

The equations for calculating the mass-based scaling factor of head kinematics are shown below. This method was consistent with the previous work in validating the DJI Phantom 3 model (1).

Mass Ratio: $\lambda_m = \frac{M_{(THUMS)}}{M_{(cadaver)}}$

Linear acceleration factor: $\lambda_a = (\lambda_m)^{\frac{-1}{3}}$

Angular velocity factor: $\lambda_\omega = (\lambda_m)^{\frac{-1}{3}}$

Predicted Head kinematics:

Linear acceleration: $a_{(cadaver)} = \frac{a_{(THUMS)}}{\lambda_a}$

Angular velocity: $\omega_{(cadaver)} = \frac{\omega_{(THUMS)}}{\lambda_\omega}$

Where, $a_{(cadaver)}$ and $a_{(THUMS)}$ represent the linear acceleration of cadaver and THUMS model; $\omega_{(cadaver)}$ and $\omega_{(THUMS)}$ represent the angular velocity of male and female.

2.2 Wood Block Model

To understand the effect of a large range of changing velocities and kinetic energy, a simple wood block FE model was developed according to ASSURE experiment and then validated against experimental data. The wood block was also used in experiments to investigate its interaction with the head. Then a parametric study with impact velocities ranging from 20 to 80 ft/s (6.10 – 24.38 m/s) were simulated.

The wood block impacts as described in the ASSURE report were conducted using three different experimental setups, which involved the analysis of impacts at velocities of 20, 30, and 40 ft/s. In this study, we aimed to verify the linear acceleration and rotational velocity results predicted by the FE model based on the data from the ASSURE report. Subsequently, we conducted a parametric study that simulated impact velocities ranging from 20 to 80 ft/s. **Table 7** displays the initial boundary and loading conditions that were utilized to set the initial conditions of the wood block FE model in relation to the human head, as per the experimental setup described in the ASSURE report. ***Table 8*** shows impact velocities and kinetic energies of seven simulation settings.

Table 7: Cadaveric data for Validation

Case #	Impact Direction	Sex	Impact Velocity (m/s (ft/s))	Cadaver subject (Table 6)
1	Lateral	Male	6.10 (20)	5
2	Lateral	Male	9.14 (30)	5
3	Lateral	Male	12.19 (40)	5

Table 8: Wood Block Parametric Study

Case #	Impact Direction	Sex	Impact Velocity (m/s (ft/s))	Kinetic Energy (J)
1	Lateral	Male	6.10 (20)	22.8
2	Lateral	Male	9.14 (30)	50.78
3	Lateral	Male	12.19 (40)	91.18
4	Lateral	Male	15.24 (50)	142.28
5	Lateral	Male	18.30 (60)	205.1
6	Lateral	Male	21.34 (70)	277.8
7	Lateral	Male	24.38 (80)	364.6

The FE model of the wood block and the THUMS 50th percentile male model is illustrated in **Figure 5**. The wood block model that was meshed using LS-PrePost is depicted in **Figure 5** (c). Modeling wood materials in LS-PrePost presents a significant challenge as there is no direct material available that accurately captures the behavior of wood. To overcome this, we referred to the manual for LS-DYNA, specifically the Wood Material Model 143, which provides a detailed description of Southern Yellow Pine wood material. Using this description, we implemented a Piecewise Linear Plasticity card to define the material property of wood.

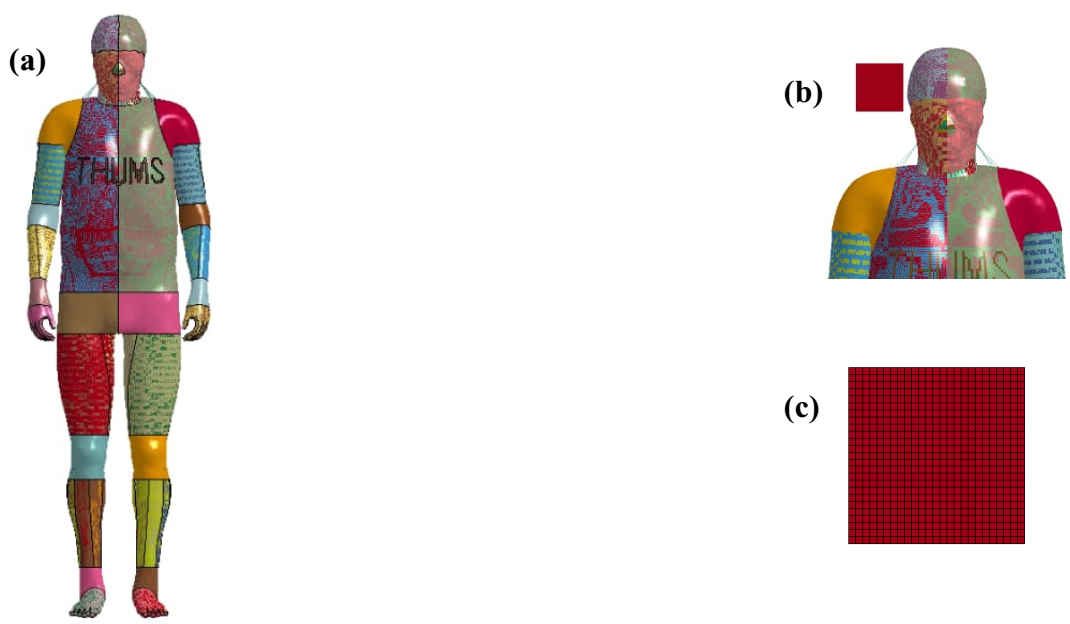

Figure 5: a) THUMS 50th Percentile Male b) Wood Block Setting c) Wood Block Model

2.3 Comprehensive comparison of head responses among various populations and between two types of sRPA

2.3.1 Comparison among various populations

In this report, the head responses of various populations including average male, small female, 10 YO child, 6 YO child, and 3 YO child are summarized and compared. In this comparison, data from previous years was included (1, 2).

2.3.2 Comparison between two types of sRPA

In this report, the head responses to the DJI Phantom 3 and DJI Mavic Pro during head impacts are summarized and compared. In this comparison, data from previous years was included (1, 2).

3 RESULTS

3.1 DJI Mavic Pro Development and Validation

3.1.1 DJI Mavic Pro Finite Element Model

A representative quadcopter style DJI Mavic Pro FE model was developed (**Figure 6**). The FE model was made up of various structural parts, including chassis upper portion, chassis lower portion, sRPA frame, battery, propeller assembly, arms, and camera assembly. In total, the FE model was made up of 56,512 1D and 2D elements, including 961 1D beam elements and 55,551 2D shell elements. In total, the model has a mass of 1.641 lbs (744 g), which is 1.2% heavier when compared to the physical model. This is deemed to be an acceptable variance.

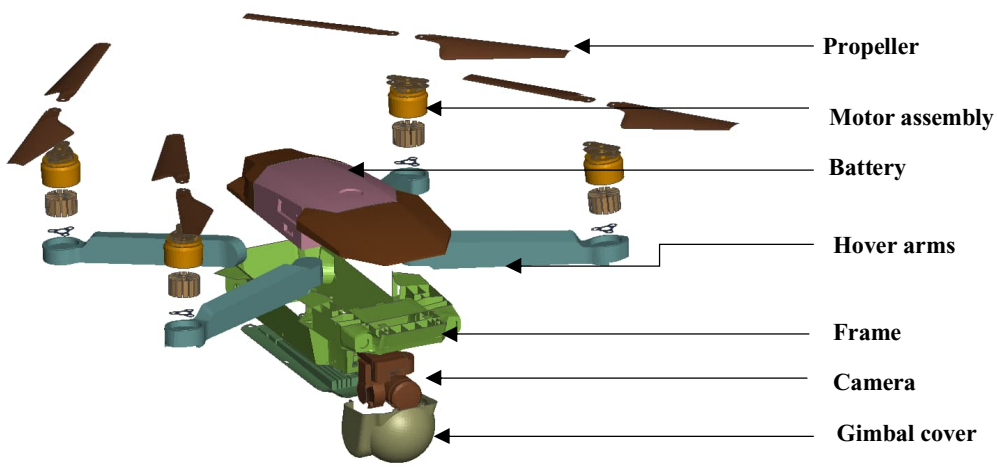

Figure 6: DJI Mavic Pro finite element model details (Exploded View)

High quality meshes were used in this model to ensure accuracy. Shell elements include 55,147 2D quad elements representing 99.27% of all shell elements, and 404 2D triangle elements

representing 0.037% of all shell elements. For 2D shell elements, 3% of elements had a warpage value greater than 5 with maximum value of 46.45. All 2D shell elements had aspect ratios below 5. A total of 3% of 2D elements had a Jacobian value smaller than 0.7 with the minimum value of 0.43. All 2D elements had elements length greater than 1mm with minimum length of 1.07 mm and with maximum length of 3.86 mm. Besides ensuring mesh qualities, the dimensions of the FE model were verified based on the DJI Mavic Pro Quadcopter dimensional specifications.

3.1.2 Validation

3.1.2.1 Resultant linear acceleration validation for DJI Mavic Pro FE model

All four head impact simulation cases, as defined according the cadaveric experiments, were validated (**Figure 7**) using frontal 58-degree sRPA impact data. During the impact, one peak in the linear acceleration appeared in all the impact cases. The impact duration was approximately 2 milliseconds. The simulated peak linear acceleration matched well with the cadaver experiments, though the simulated results slightly underestimated the peak value by around 10% in Case 1. The peak linear acceleration of simulation was approximately 8% greater than that of experiment in Case 4.

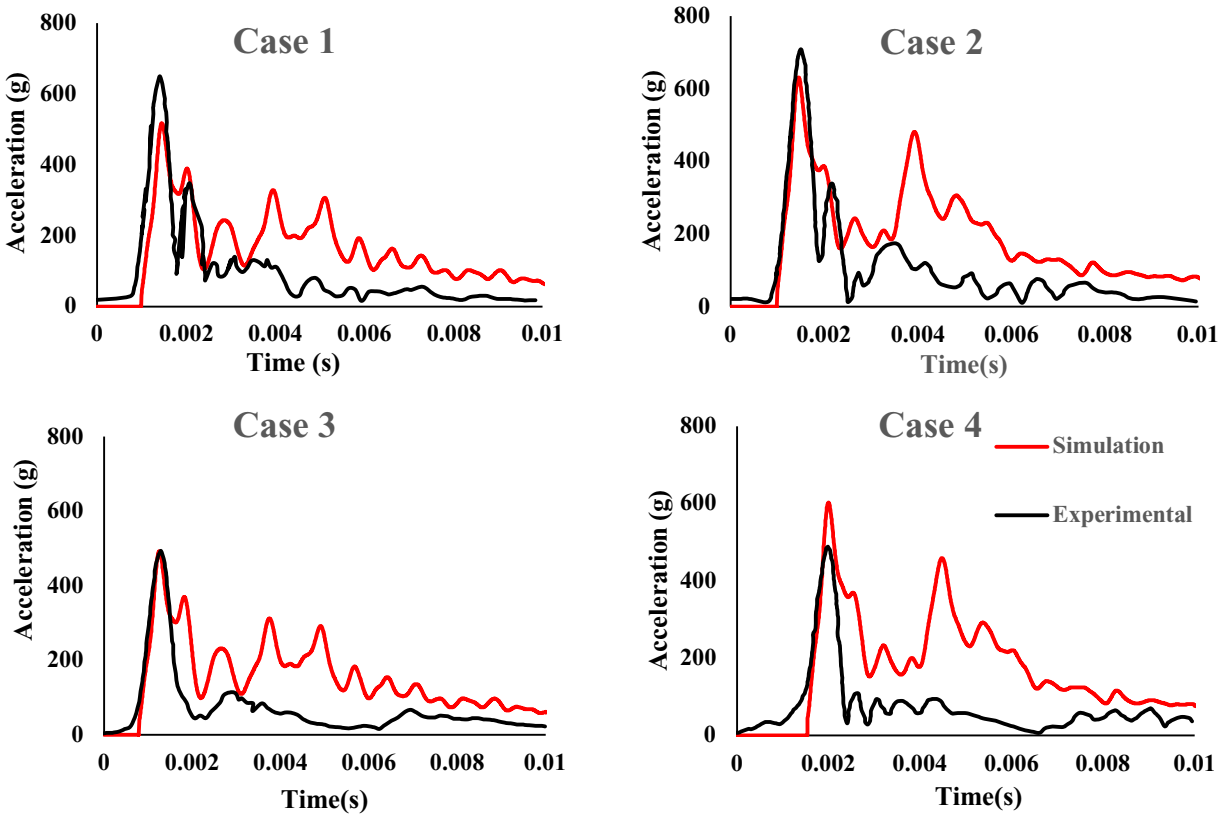

Figure 7: DJI Mavic Pro FE model validation for head linear acceleration

3.1.2.2 Resultant rotational velocity validation for DJI Mavic Pro FE model

The rotational velocity curves were compared between simulation and experiments (**Figure 8**). There were inconsistencies in cadaveric data, but model-predicted rotational velocity was in the range of experimental measurements. The peak values of simulation and experimental values were generally close in the first two cases. For the first two cases, the peak value occurred at around 16 milliseconds. However, in simulation, the rotational velocity peaked at around 5 milliseconds. In case 3 and 4, the peak rotational values were 34% and 27% higher than those of experiments.

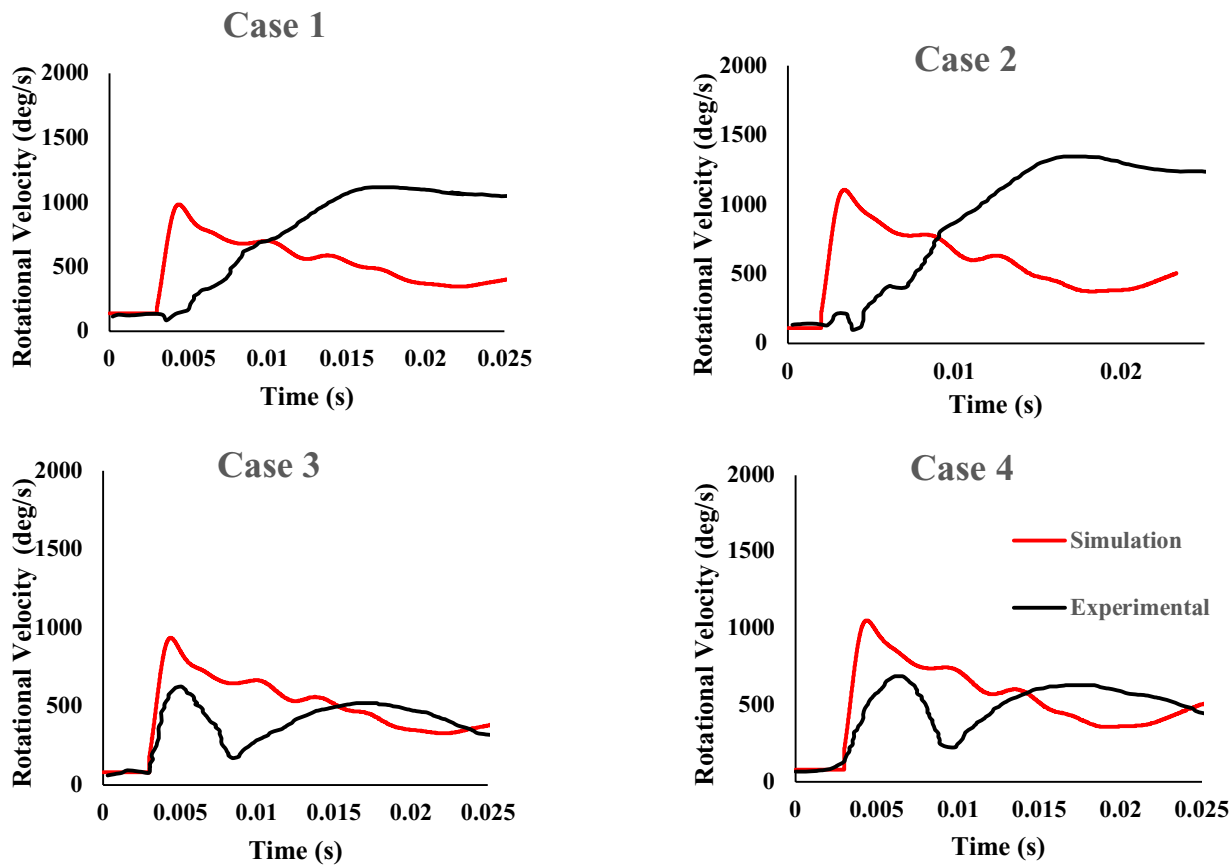

Figure 8: DJI Mavic Pro FE model comparison for head rotational velocity

3.2 Wood Block Simulation Results

3.2.1 Wood Block Model Validation

3.2.1.1 Resultant Linear Acceleration Validation

Validation was performed on all three cases defined in Table 7 using lateral wood block impacts (**Figure 9**). During impacts, a single peak linear acceleration was observed in all three cases, with

an impact duration of approximately 2 milliseconds. The simulation results for peak linear acceleration matched those from the cadaver experiments, with a slight overestimation of approximately 18% from FE prediction seen in Case 2. In Case 3, the peak linear acceleration from the simulation was approximately 27% higher than that from the experiment. For wood block experiments, only lateral impact mode is available.

3.2.1.2 Resultant Rotational Velocity Validation

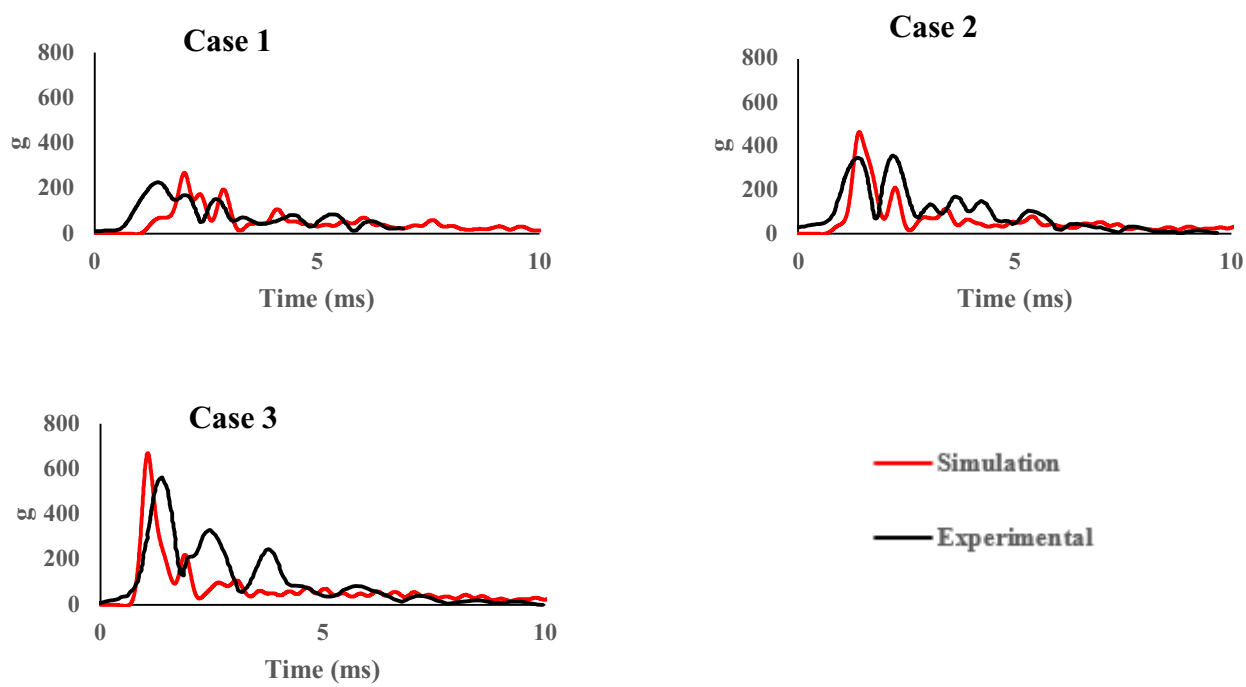

Figure 9: Wood Block FE model validation for linear acceleration

The simulation results in **Figure 10** indicate a close resemblance to the experimental cadaver outcomes in terms of peak rotational velocity during impact. However, notable differences were observed in the temporal profile of the peak resultant velocity. The experimental results demonstrate a consistent trend across all three cases, with the peak resultant velocity occurring at approximately 5 milliseconds, followed by a slight drop and a gradual increase, reaching its maximum at around 20 milliseconds and gradually decreasing thereafter. The simulation results exhibit a similar pattern, with the peak value occurring around 4 milliseconds, followed by a sudden drop, and a gradual increase leading to the maximum value at approximately 40 milliseconds. These findings suggest that although the simulation results accurately reproduce the peak rotational velocity, there are discrepancies in the temporal behavior of the resultant velocity.

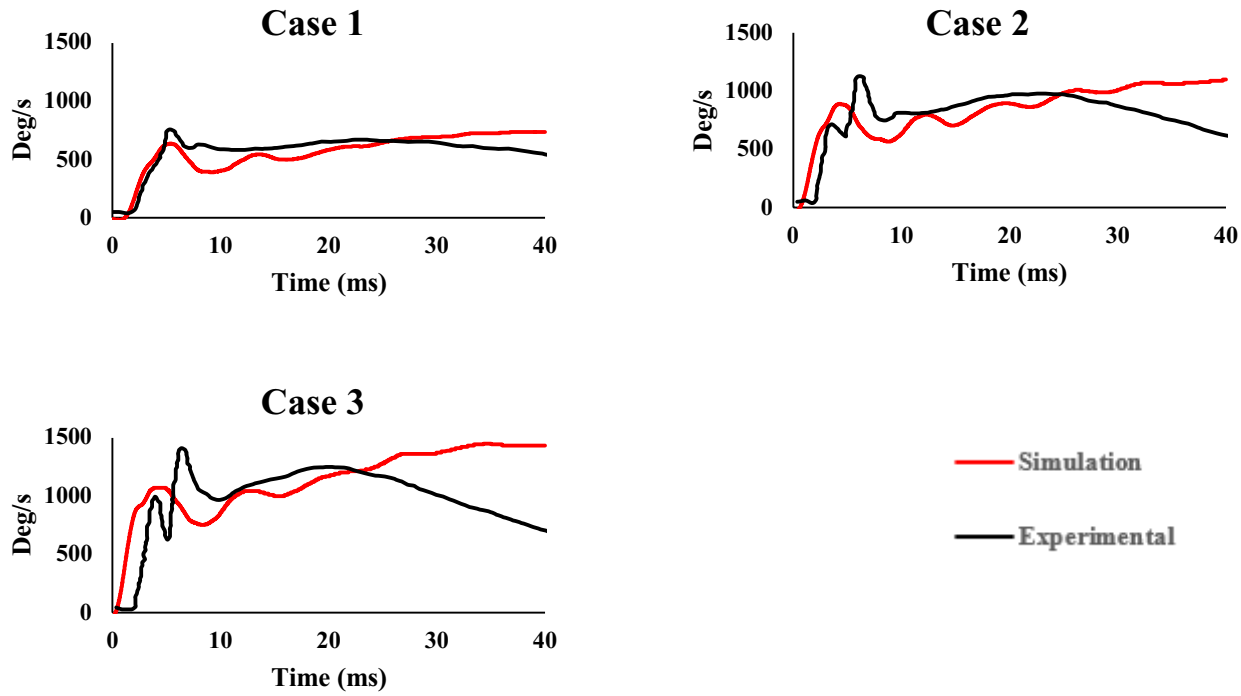

Figure 10: Wood Block FE model validation for rotational velocity

3.2.2 Correlation Analysis

There are strong correlations between impact velocity/kinetic energy and head responses. Compared to the sRPA model, the wood block model utilized in this study represents a comparatively straightforward model. This allowed researchers to conduct a parametric investigation of the impact of the wood block on the head with varying velocities while keeping the impact position constant. Analysis of the simulated data pertaining to linear acceleration revealed a consistent pattern in the graphs, but with varying peak values. Also, our findings indicate a significant correlation between impact velocity/kinetic energy and the resulting response of the head.

Figure 11 shows that there is a significant correlation between wood block impact velocity and head linear acceleration, with an R^2 value of 0.97. **Figure 12** shows there is a significant correlation between wood block impact velocity and head rotational velocity, with an R^2 value of 0.99.

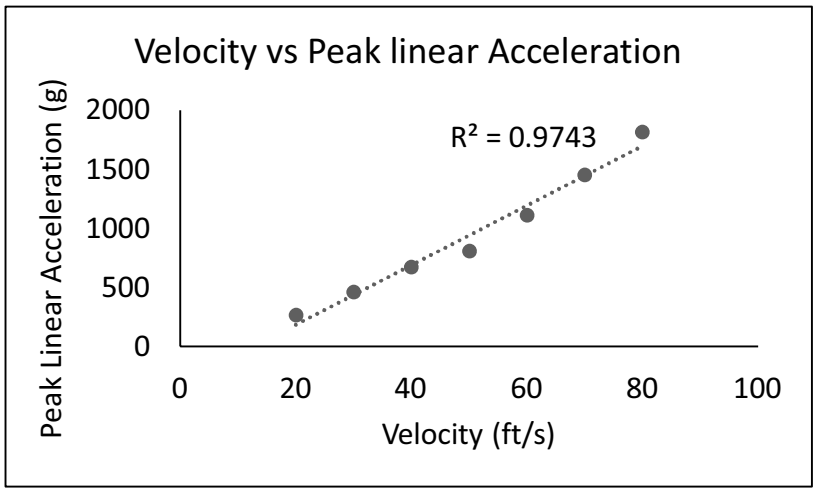

Figure 11: Correlation between wood block impact velocity and linear acceleration

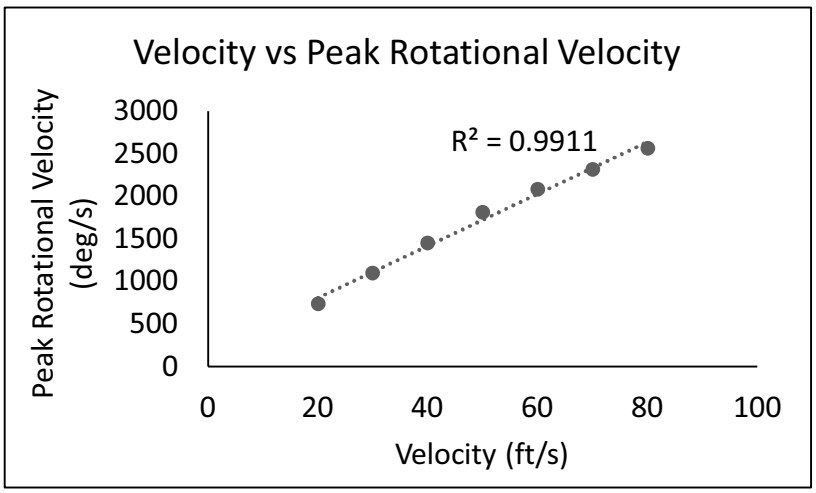

Figure 12: Correlation between wood block impact velocity and rotational velocity

Figure 13 shows that there is a significant correlation between wood block impact velocity and head injury criteria (HIC), with an R^2 value of 0.99. **Figure 14** shows that there is a significant correlation between wood block impact velocity and brain injury criteria (BrIC), with an R^2 value of 0.97.

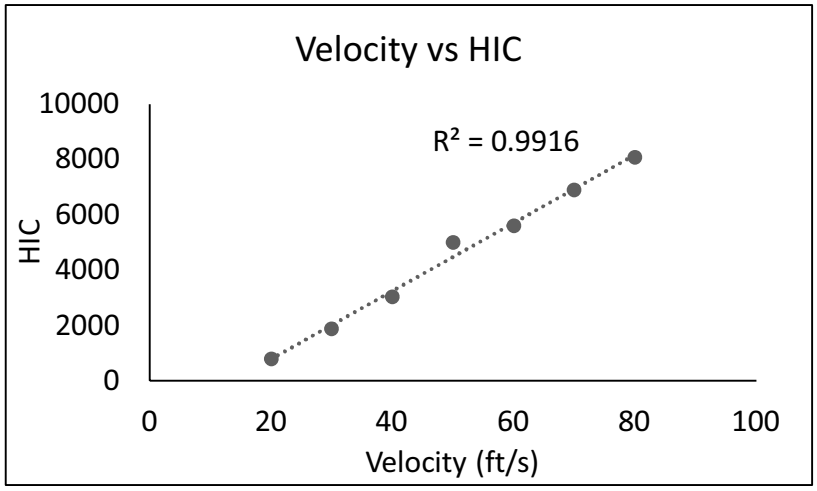

Figure 13: Correlation between wood block impact velocity and HIC

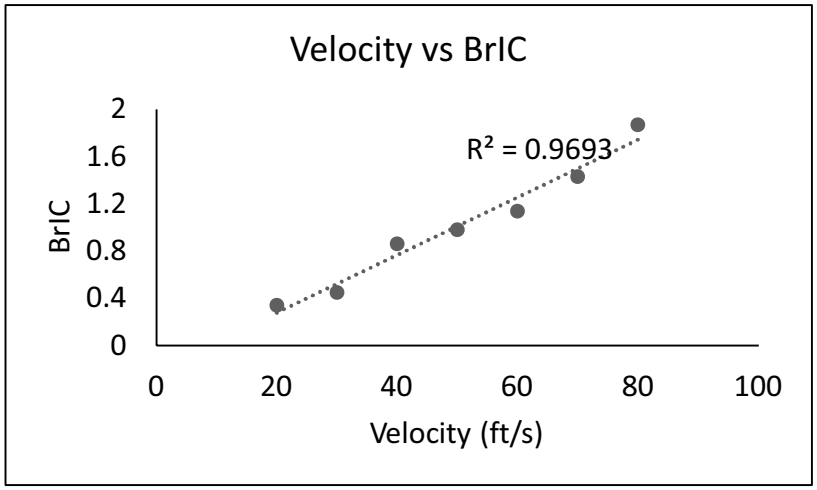

Figure 14: Correlation between wood block impact velocity and BrIC

In terms of kinetic energy, there are significant correlations to BrIC (**Figure 15**), rotational velocity (**Figure 16**), linear acceleration (**Figure 17**) and HIC (**Figure 18**).

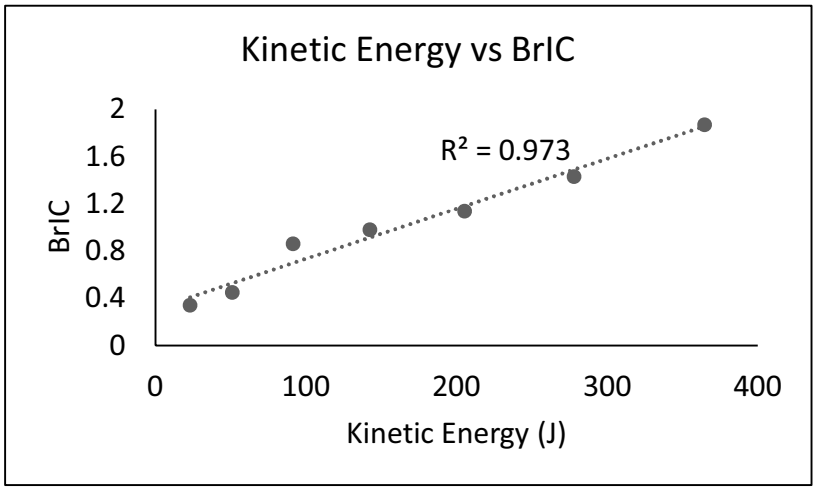

Figure 15: Correlation between kinetic energy and BrIC

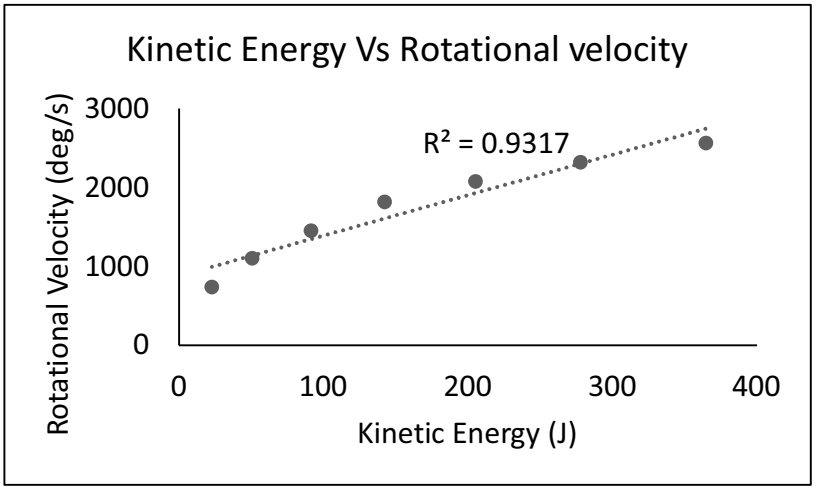

Figure 16: Correlation between kinetic energy and rotational velocity

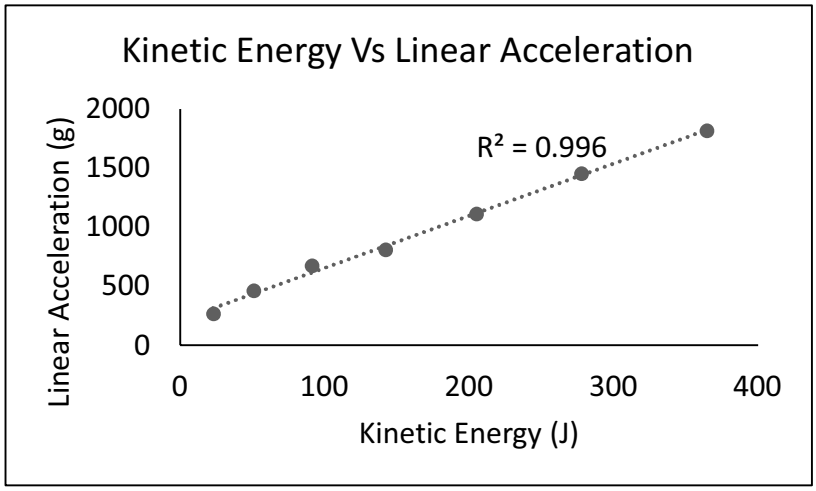

Figure 17: Correlation between kinetic energy and linear acceleration

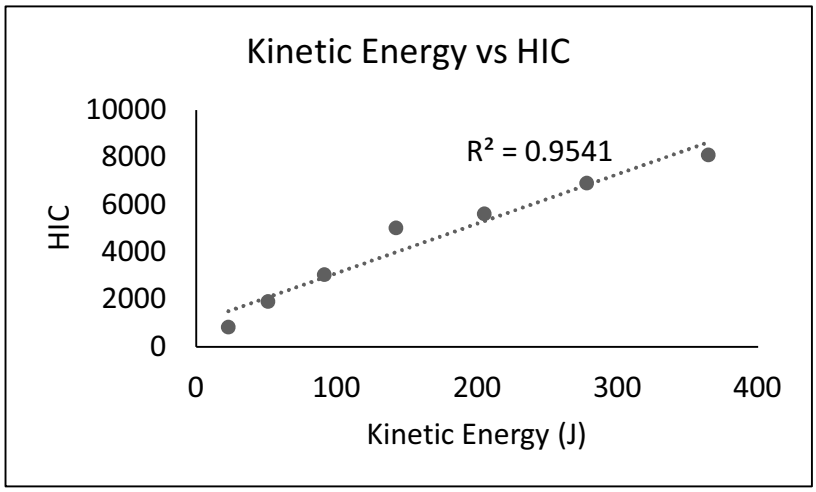

Figure 18: Correlation between kinetic energy and HIC

3.3 Comprehensive Comparison

3.3.1 Comparisons Across Populations

The current study compared male, female, and child populations with impacts with the DJI Phantom 3, and the results are shown in the tables below. We specifically assessed peak linear acceleration, rotational velocity, HIC, BrIC, and skull stress, with the comparative results given in the tables. Specifically, the differences across populations were investigated and documented.

Table 9 to Table 25 summarize differences of adult male, small female, 10 YO child, 6 YO child and 3 YO child under the different impact settings scenarios analyzed in this study.

One of the most prominent results is that HIC, as well as linear acceleration, show a strong population-based effect. For example, in **Table 9**, the predicted HIC value was 1311 for an average male, 3105 for small female, 5816 for 10 YO child, 4537 for 6 YO child, and 5543 for 3 YO child. Although the differences of HIC between small female and 10 YO were not always consistent, the trend of increasing HIC with decreasing body height/mass (from average male to small female, to 10, 6 and 3 YO children) was clear. As HIC is associated with linear acceleration, the similar increasing trend was found.

For BrIC, it is shown that small female and children would experience higher BrIC under the same impact condition. For example, BrIC values are 0.43, 0. 73, 0.87, 0.84, and 0.77 for average male, small female, 10 YO, 6 YO, and 3 YO, respectively (**Table 9**). Overall, the BrIC values increased for children compared to the adult male.

Interestingly, maximum skull stress values varied and did not show a clear trend overall. For example, under lateral 0-degree impact, the average male experienced a skull stress of 71 MPa, the small female experienced a skull stress of 81 MPa, the 10 YO child experienced a skull stress of 107 MPa, the 6 YO child experienced a skull stress of 92 MPa, and the 3 YO experienced a skull stress of 58 MPa (**Table 9**). During a frontal 58-degree impact, the average male experienced a skull stress of 102 MPa, the small female experienced a skull stress of 97 MPa, the 10 YO child experienced a skull stress of 79 MPa, the 6 YO child experienced a skull stress of 77 MPa, and the 3 YO experienced a skull stress of 59 MPa (**Table 12**).

Table 9: Case-1 (Phantom 3) - Lateral 0-degree impact at a velocity of 56 ft/s

OSU 2: Lateral 0 Degree									
Subject	sRPA Speed (ft/s)	ASSURE Cadaver HIC	Simulated HIC	Peak Cadaver Lin Resultant Acceleration (g)	Peak Simulation Lin Resultant Acceleration (g)	Peak Cadaver Rot Vel (deg/s)	Peak simulation Rot Vel (deg/s)	Simulation BrIC	Simulation Maximum Skull Stress
Male 50th	56	866	1311	159.1	284	1282	1467	0.43	71.0
Female 5th		N/A	3105	N/A	454	N/A	2328	0.73	81.2
Child 10YO		N/A	5816	N/A	532	N/A	3090	0.87	107.3
Child 6YO		N/A	4537	N/A	508	N/A	2966	0.84	91.6
Child 3YO		N/A	5543	N/A	492	N/A	2786	0.77	58.5

Table 10: Case-2 (Phantom 3) - Lateral 0-degree impact at a velocity of 61 ft/s

OSU 3: Lateral 0 Degree									
Subject	sRPA Speed (ft/s)	ASSURE Cadaver HIC	Simulated HIC	Peak Cadaver Lin Resultant Acceleration (g)	Peak Simulation Lin Resultant Acceleration (g)	Peak Cadaver Rot Vel (deg/s)	Peak simulation Rot Vel (deg/s)	Simulation BrIC	Simulation Maximum Skull Stress
Male 50th	61	535	1800	328	354	1717	1581	0.46	77.6
Female 5th		N/A	3817	N/A	498	N/A	2599	0.80	85.6
Child 10YO		N/A	7000	N/A	591	N/A	3239	0.91	115.0
Child 6YO		N/A	5895	N/A	577	N/A	3144	0.89	109.1
Child 3YO		N/A	6714	N/A	515	N/A	2962	0.82	59.2

Table 11: Case-3 (Phantom 3) - Lateral 0-degree impact at a velocity of 71 ft/s

OSU 4: Lateral 0 Degree									
Subject	sRPA Speed (ft/s)	ASSURE Cadaver HIC	Simulated HIC	Peak Cadaver Lin Resultant Acceleration (g)	Peak Simulation Lin Resultant Acceleration (g)	Peak Cadaver Rot Vel (deg/s)	Peak simulation Rot Vel (deg/s)	Simulation BrIC	Simulation Maximum Skull Stress
Male 50th	71	2892	2380	487	391	1903	1730	0.49	83.9
Female 5th		N/A	5488	N/A	556	N/A	2216	0.72	96.6
Child 10YO		N/A	9521	N/A	669	N/A	3553	1.00	119.4
Child 6YO		N/A	9109	N/A	691	N/A	3450	0.99	90.8
Child 3YO		N/A	9389	N/A	588	N/A	3171	0.88	59.4

Table 12: Case-4 (Phantom 3) - Frontal 58-degree impact at a velocity of 56 ft/s

OSU 6: Frontal 58 Degree									
Subject	sRPA Speed (ft/s)	ASSURE Cadaver HIC	Simulated HIC	Peak Cadaver Lin Resultant Acceleration (g)	Peak Simulation Lin Resultant Acceleration (g)	Peak Cadaver Rot Vel (deg/s)	Peak simulation Rot Vel (deg/s)	Simulation BrIC	Simulation Maximum Skull Stress
Male 50th	56	522	690	220	213	1352	1017	0.32	102.0
Female 5th		N/A	1459	N/A	282	N/A	1319	0.41	97.0
Child 10YO		N/A	1418	N/A	268	N/A	2903	0.90	78.5
Child 6YO		N/A	2917	N/A	427	N/A	2986	0.92	77.1
Child 3YO		N/A	4263	N/A	475	N/A	3499	1.08	58.8

Table 13: Case-5 (Phantom 3) - Frontal 58-degree impact at a velocity of 61 ft/s

OSU 7: Frontal 58 Degree									
Subject	sRPA Speed (ft/s)	ASSURE Cadaver HIC	Simulated HIC	Peak Cadaver Lin Resultant Acceleration (g)	Peak Simulation Lin Resultant Acceleration (g)	Peak Cadaver Rot Vel (deg/s)	Peak simulation Rot Vel (deg/s)	Simulation BrIC	Simulation Maximum Skull Stress
Male 50th	61	1304	757	241	220	1605	1075	0.33	100.0
Female 5th		N/A	1611	N/A	291	N/A	1407	0.44	112.0
Child 10YO		N/A	1590	N/A	281	N/A	3061	0.95	76.4
Child 6YO		N/A	3040	N/A	434	N/A	3053	0.94	74.5
Child 3YO		N/A	4296	N/A	476	N/A	3508	1.09	61.8

Table 14: Case-6 (Phantom 3) - Frontal 58-degree impact at a velocity of 61 ft/s

OSU 8a: Frontal 58 Degree									
Subject	sRPA Speed (ft/s)	ASSURE Cadaver HIC	Simulated HIC	Peak Cadaver Lin Resultant Acceleration (g)	Peak Simulation Lin Resultant Acceleration (g)	Peak Cadaver Rot Vel (deg/s)	Peak simulation Rot Vel (deg/s)	Simulation BrIC	Simulation Maximum Skull Stress
Male 50th	61	380	749	159	218	1282	1067	0.33	104.0
Female 5th		N/A	1169	N/A	254	N/A	2742	0.85	86.7
Child 10YO		N/A	1482	N/A	278	N/A	2981	0.92	71.5
Child 6YO		N/A	3015	N/A	434	N/A	3067	0.95	68.0
Child 3YO		N/A	4410	N/A	486	N/A	3536	1.09	61.8

Table 15: Case-7 (Phantom 3) - Frontal 58-degree impact at a velocity of 71 ft/s

OSU 9: Frontal 58 Degree									
Subject	sRPA Speed (ft/s)	ASSURE Cadaver HIC	Simulated HIC	Peak Cadaver Lin Resultant Acceleration (g)	Peak Simulation Lin Resultant Acceleration (g)	Peak Cadaver Rot Vel (deg/s)	Peak simulation Rot Vel (deg/s)	Simulation BrIC	Simulation Maximum Skull Stress
Male 50th	71	539	543	176	194	1444	1393	0.43	107.0
Female 5th		N/A	1169	N/A	254	N/A	2742	0.85	86.7
Child 10YO		N/A	1365	N/A	297	N/A	2837	0.88	75.0
Child 6YO		N/A	3190	N/A	454	N/A	3207	0.99	71.9
Child 3YO		N/A	4846	N/A	537	N/A	3734	1.16	57.8

Table 16: Case-8 (Phantom 3) - Lateral 58-degree impact at a velocity of 61 ft/s

OSU 10: Lateral 58 Degree									
Subject	sRPA Speed (ft/s)	ASSURE Cadaver HIC	Simulated HIC	Peak Cadaver Lin Resultant Acceleration (g)	Peak Simulation Lin Resultant Acceleration (g)	Peak Cadaver Rot Vel (deg/s)	Peak simulation Rot Vel (deg/s)	Simulation BrIC	Simulation Maximum Skull Stress
Male 50th	61	500	1669	237	303	992	1398	0.41	62.3
Female 5th		N/A	2961	N/A	395	N/A	1723	0.63	72.3
Child 10YO		N/A	4888	N/A	474	N/A	3539	0.99	89.8
Child 6YO		N/A	5228	N/A	478	N/A	2860	0.80	87.8
Child 3YO		N/A	5851	N/A	549	N/A	3381	0.95	59.3

Table 17: Case-9 (Phantom 3) - Lateral 58-degree impact at a velocity of 71 ft/s

OSU 11a: Lateral 58 Degree									
Subject	sRPA Speed (ft/s)	ASSURE Cadaver HIC	Simulated HIC	Peak Cadaver Lin Resultant Acceleration (g)	Peak Simulation Lin Resultant Acceleration (g)	Peak Cadaver Rot Vel (deg/s)	Peak simulation Rot Vel (deg/s)	Simulation BrIC	Simulation Maximum Skull Stress
Male 50th	71	929	2074	302	364	1342	1556	0.44	76.3
Female 5th		N/A	3638	N/A	443	N/A	1912	0.68	111.0
Child 10YO		N/A	5926	N/A	492	N/A	3539	0.99	89.8
Child 6YO		N/A	5135	N/A	477	N/A	2877	0.81	75.7
Child 3YO		N/A	7509	N/A	591	N/A	3810	1.07	55.5

Table 18: Case-10 (Phantom 3) - Top 90-degree impact at a velocity of 56 ft/s

OSU 13: Top 90 Degree									
Subject	sRPA Speed (ft/s)	ASSURE Cadaver HIC	Simulated HIC	Peak Cadaver Lin Resultant Acceleration (g)	Peak Simulation Lin Resultant Acceleration (g)	Peak Cadaver Rot Vel (deg/s)	Peak simulation Rot Vel (deg/s)	Simulation BrIC	Simulation Maximum Skull Stress
Male 50th	56	1848	1138	391	272	1121	931	0.29	26.5
Female 5th		N/A	2053	N/A	331	N/A	1097	0.34	29.5
Child 10YO		N/A	4057	N/A	431	N/A	1227	0.38	62.0
Child 6YO		N/A	3809	N/A	487	N/A	1651	0.51	55.1
Child 3YO		N/A	4778	N/A	475	N/A	1194	0.37	56.0

Table 19: Case-11 (Phantom 3) - Top 90-degree impact at a velocity of 65 ft/s

OSU 14: Top 90 Degree									
Subject	sRPA Speed (ft/s)	ASSURE Cadaver HIC	Simulated HIC	Peak Cadaver Lin Resultant Acceleration (g)	Peak Simulation Lin Resultant Acceleration (g)	Peak Cadaver Rot Vel (deg/s)	Peak simulation Rot Vel (deg/s)	Simulation BrIC	Simulation Maximum Skull Stress
Male 50th	65	2550	1481	467	298	1092	897	0.28	25.8
Female 5th		N/A	2550	N/A	336	N/A	1101	0.34	29.5
Child 10YO		N/A	4862	N/A	454	N/A	1198	0.37	46.0
Child 6YO		N/A	4758	N/A	515	N/A	1814	0.56	53.9
Child 3YO		N/A	6158	N/A	565	N/A	1419	0.44	62.9

Table 20: Case-12 (Phantom 3) - Top 90-degree impact at a velocity of 71 ft/s

OSU 15: Top 90 Degree									
Subject	sRPA Speed (ft/s)	ASSURE Cadaver HIC	Simulated HIC	Peak Cadaver Lin Resultant Acceleration (g)	Peak Simulation Lin Resultant Acceleration (g)	Peak Cadaver Rot Vel (deg/s)	Peak simulation Rot Vel (deg/s)	Simulation BrIC	Simulation Maximum Skull Stress
Male 50th	71	4197	1957	551	317	693	777	0.24	66.7
Female 5th		N/A	2989	N/A	355	N/A	992	0.31	38.2
Child 10YO		N/A	5384	N/A	464	N/A	1097	0.34	46.4
Child 6YO		N/A	5552	N/A	536	N/A	1816	0.56	58.2
Child 3YO		N/A	7144	N/A	600	N/A	1661	0.52	65.5

Table 21: Case-13 (Phantom 3) - Lateral 58-degree impact at a velocity of 61 ft/s

OSU 16: Lateral 58 Degree									
Subject	sRPA Speed (ft/s)	ASSURE Cadaver HIC	Simulated HIC	Peak Cadaver Lin Resultant Acceleration (g)	Peak Simulation Lin Resultant Acceleration (g)	Peak Cadaver Rot Vel (deg/s)	Peak simulation Rot Vel (deg/s)	Simulation BrIC	Simulation Maximum Skull Stress
Male 50th	61	401	1652	218	337	1046	1473	0.40	72.6
Female 5th		N/A	2979	N/A	408	N/A	1784	0.64	57.3
Child 10YO		N/A	4851	N/A	472	N/A	3111	0.87	106.5
Child 6YO		N/A	5135	N/A	477	N/A	2860	0.80	87.8
Child 3YO		N/A	5828	N/A	552	N/A	3386	0.44	58.5

Table 22: Case-14 (Phantom 3) - Lateral 58-degree impact at a velocity of 71 ft/s

OSU 17: Lateral 58 Degree									
Subject	sRPA Speed (ft/s)	ASSURE Cadaver HIC	Simulated HIC	Peak Cadaver Lin Resultant Acceleration (g)	Peak Simulation Lin Resultant Acceleration (g)	Peak Cadaver Rot Vel (deg/s)	Peak simulation Rot Vel (deg/s)	Simulation BrIC	Simulation Maximum Skull Stress
Male 50th	71	2527	2233	378	371	1386	1812	0.51	86.8
Female 5th		N/A	4057	N/A	443	N/A	2509	0.78	86.8
Child 10YO		N/A	5926	N/A	492	N/A	3539	0.99	89.8
Child 6YO		N/A	5135	N/A	477	N/A	2877	0.81	75.7
Child 3YO		N/A	7509	N/A	591	N/A	3810	1.07	71.2

Table 23: Case-15 (Phantom 3) - Frontal 58-degree impact at a velocity of 71 ft/s

OSU 19: Frontal 58 Degree									
Subject	sRPA Speed (ft/s)	ASSURE Cadaver HIC	Simulated HIC	Peak Cadaver Lin Resultant Acceleration (g)	Peak Simulation Lin Resultant Acceleration (g)	Peak Cadaver Rot Vel (deg/s)	Peak simulation Rot Vel (deg/s)	Simulation BrIC	Simulation Maximum Skull Stress
Male 50th	71	5473	2124	387	371	1443	1409	0.44	127.0
Female 5th		N/A	3030	N/A	383	N/A	1755	0.54	81.8
Child 10YO		N/A	1391	N/A	302	N/A	2852	0.88	60.5
Child 6YO		N/A	3170	N/A	448	N/A	3229	1.00	71.4
Child 3YO		N/A	4901	N/A	555	N/A	3770	1.17	58.3

Table 24: Case-16 (Phantom 3) - Top 90-degree impact at a velocity of 65 ft/s

OSU 22: Top 90 Degree									
Subject	sRPA Speed (ft/s)	ASSURE Cadaver HIC	Simulated HIC	Peak Cadaver Lin Resultant Acceleration (g)	Peak Simulation Lin Resultant Acceleration (g)	Peak Cadaver Rot Vel (deg/s)	Peak simulation Rot Vel (deg/s)	Simulation BrIC	Simulation Maximum Skull Stress
Male 50th	65	1219	1482	357	295	865	1069	0.27	25.6
Female 5th		N/A	2502	N/A	344	N/A	1111	0.34	28.7
Child 10YO		N/A	4841	N/A	451	N/A	1172	0.36	42.7
Child 6YO		N/A	4757	N/A	514	N/A	1816	0.56	45.3
Child 3YO		N/A	6212	N/A	564	N/A	1389	0.43	61.5

Table 25: Case-17 (Phantom 3) - Top 90-degree impact at a velocity of 71 ft/s

OSU 22: Top 90 Degree									
Subject	sRPA Speed (ft/s)	ASSURE Cadaver HIC	Simulation HIC	Peak Cadaver Lin Resultant Acceleration (g)	Peak Simulation Lin Resultant Acceleration (g)	Peak Cadaver Rot Vel (deg/s)	Peak simulation Rot Vel (deg/s)	Simulation BrIC	Simulation Maximum Skull Stress
Male 50th	71	1748	1987	308	321	1110	780	0.24	65.8
Female 5th		N/A	2301	N/A	329	N/A	557	0.18	29.2
Child 10YO		N/A	5386	N/A	464	N/A	1097	0.34	46.4
Child 6YO		N/A	5552	N/A	536	N/A	1816	0.56	52.1
Child 3YO		N/A	7144	N/A	600	N/A	1660	0.52	65.5

3.3.2 Comparisons Between Two Types of sRPA

Table 26 and **Table 27** show a comparison between two studied types of sRPA. For the second type of sRPA (DJI Mavic Pro), as cadaver data was only available for frontal 58-degree impact, the validation and comparison were only done at this impact setting.

One interesting finding is that, although the DJI Mavic Pro is lighter than the DJI Phantom 3, its impact with the human head causes higher HIC and linear acceleration values across all populations.

Table 26: Mavic vs Phantom- Frontal 58-Degree impact at a velocity of 61 ft/s

Subject	ASSURE Cadaver HIC		Simulation HIC		Peak Cadaver Lin Res (g)		Peak Simulation Lin Res (g)		Peak Cadaver Rot Vel (deg/s)		Peak Simulation Rot Vel (deg/s)		Simulation BrIC		ASSURE Cadaver BrIC	
	Mavic Pro	Phantom 3	Mavic Pro	Phantom 3	Mavic Pro	Phantom 3	Mavic Pro	Phantom 3	Mavic Pro	Phantom 3	Mavic Pro	Phantom 3	Mavic Pro	Phantom 3	Mavic Pro	Phantom 3
Male 50th	1740	380	1440	749	502	159	473	218	627	1282	809	1067	0.339	0.332	0.25	N/A
Female 5th	N/A	N/A	1890	1169	N/A	N/A	498	254	N/A	N/A	1987	2742	0.786	0.849	N/A	N/A
Child 10YO	N/A	N/A	2665	1482	N/A	N/A	546	278	N/A	N/A	3123	2981	0.987	0.923	N/A	N/A
Child 6YO	N/A	N/A	4186	3015	N/A	N/A	602	434	N/A	N/A	4451	3067	1.09	0.948	N/A	N/A
Child 3YO	N/A	N/A	5027	4410	N/A	N/A	681	486	N/A	N/A	4986	3536	1.19	1.09	N/A	N/A

Table 27:Mavic vs Phantom- Frontal 58-Degree impact at a velocity of 71 ft/s

Subject	ASSURE Cadaver HIC		Simulation HIC		Peak Cadaver Lin Res (g)		Peak Simulation Lin Res (g)		Peak Cadaver Rot Vel (deg/s)		Peak Simulation Rot Vel (deg/s)		Simulation BrIC		ASSURE Cadaver BrIC	
	Mavic Pro	Phantom 3	Mavic Pro	Phantom 3	Mavic Pro	Phantom 3	Mavic Pro	Phantom 3	Mavic Pro	Phantom 3	Mavic Pro	Phantom 3	Mavic Pro	Phantom 3	Mavic Pro	Phantom 3
Male 50th	1927	539	2667	543	655	176	571	194	607	1444	1113	1393	0.377	0.431	0.21	N/A
Female 5th	N/A	N/A	2882	1169	N/A	N/A	598	254	N/A	N/A	1657	2742	0.897	0.849	N/A	N/A
Child 10YO	N/A	N/A	3970	1365	N/A	N/A	609	297	N/A	N/A	2565	2837	1.01	0.878	N/A	N/A
Child 6YO	N/A	N/A	5043	3190	N/A	N/A	672	454	N/A	N/A	3398	3207	1.15	0.991	N/A	N/A
Child 3YO	N/A	N/A	6944	4846	N/A	N/A	779	537	N/A	N/A	4431	3734	1.23	1.155	N/A	N/A

4 DISCUSSION AND CONCLUSION

Model development and validation – One of main challenges of developing this second sRPA model (DJI Mavic Pro) was the relatively limited cadaveric data being available compared to those available for the first sRPA model (DJI Phantom 3). However, using the data from the ASSURE report, it could be justified that a high-quality sRPA model was appropriately developed. Furthermore, great efforts were spent to ensure that the DJI Mavic Pro FE model was developed using high-quality meshes. With well-defined material properties, thickness of shell, mass of battery and the entire sRPA structures being carefully defined, it is justified that the DJI Mavic Pro FE model was of sufficiently high quality to study sRPA-to-head impacts and head injury responses. The sRPA studied in this report are commonly used by Canadian users at the time this study was conducted. This FE sRPA model, to the best of our knowledge, is the first one in the field. Together with the previous sRPA model, it is now feasible to further study how various sRPA could affect head responses of adult male and vulnerable populations under complex impact settings in the near future.

Vulnerable populations and protection – The data investigated over the years provided some very useful references when considering protecting the general public, including vulnerable populations. The extremely high HIC values at an order of magnitude in the thousands observed for vulnerable populations are especially noteworthy. In addition, the impact from a lighter sRPA to a human head caused a higher value of HIC. The lighter sRPA has less kinetic energy than a heavier sRPA under the same impact conditions but causes more HIC to a human head. This result challenges the current practice of relying purely on kinetic energy to evaluate human injury severity.

Effect of structure and use of wood block – The different head responses observed between the DJI Phantom 3 and DJI Mavic Pro highlighted the importance of sRPA structure. Despite the smaller mass, the DJI Mavic Pro induced larger head accelerations. It was postulated that the DJI Mavic Pro's side body, with a battery inside, represents a stiffer structure, while the DJI Phantom 3's shell represents a softer structure with the battery away from the head impact location. The wood block model was acknowledged as effective in demonstrating a positive relationship between kinetic energy and head kinematics. It is suggested that we investigate the structural differences between sRPA and wood blocks and understand that such structural differences could have greatly impacted head responses in the simulations.

Remaining questions and future work – There are several important unknowns that could be addressed to facilitate better human protection in the future.
1) It is shown that the shape and mass of the head affected head responses, and individual head differences have been reported and documented in the literature. How could these **individual anatomical differences** affect the results of this study? Such effects could be investigated and quantified.
2) The structures of sRPA were clearly shown to have a dramatic effect on head responses, as a lighter sRPA resulted in higher HIC, indicating the effect of structural components and stiffness. These **structural effects** need to be further studied and quantified for improved protection.
3) **HIC** or **head response at tissue level**: It is interesting that for small children, even though HIC indicates an extremely high head injury risk with values up to four thousand, the skull stress level is comparable to that of an adult who has a much lower HIC at one thousand level. Hence, the application of HIC, especially to vulnerable populations, needs to be used with great caution and needs to be further investigated.
4) **Human** vs. **dummy**. It needs to be acknowledged that this study was focused on human head responses, which are helpful for research purposes, while in current regulatory activities, physical dummies are commonly used. The differences between the human and dummy could be quantified and documented to better guide regulation development.
5) Real-world, **various impact** situations. The studied impact settings were defined according to cadaveric experiments. Due to limited availability, cadaveric experiments were conducted at several studied settings that could represent the most probable or most damaging scenarios, which is commended. However, computational models developed during this project provide a platform allowing the study of many more impacts at various angles and velocities. This work can be pursued, and the results documented to more comprehensively assess head responses under these various impact conditions, hence supporting regulation development.
6) **Vulnerable population risk**. The current results suggest a mixed trend of injury risks for the vulnerable population (small females and children) compared to an average male under the same

sRPA-to-head impact conditions. Looking purely at the HIC, the vulnerable population has a high risk of head injury as the HIC values for the small female and children models were shown to be higher under the same impact conditions. However, the skull stress values for the vulnerable population were not higher or even lower compared to an average male. Although this discrepancy remains to be further investigated, it could be postulated that given the damage to the skull must necessarily be initiated at a tissue level, the vulnerable population does not necessarily have a higher risk of skull fracture under the same impact conditions.

References

1. Weng Y, Bian K, Gunasekaran K, Gholipour J, Vidal C, Mao H. Modeling small remotely piloted aircraft system to head impact for investigating craniocerebral response. Journal of biomechanics. 2021;128:110748.

2. Weng Y, Bian K, Gunasekaran K, Gholipour J, Vidal C, Mao H. Investigating small RPAS ground impact injury severity criteria (phase 1 report). 2022.

3. Olivares G, Bolte J, Prabhu R, Duma S. Task A14: UAS Ground Collision Severity Evaluation. The FAA's Center of Excellence for UAS Research - Alliance for System Safety of UAS through Research Excellence (ASSURE); 2019.